

# The estimation of the SZ effects with unbiased multifilters

D. Herranz<sup>1\*</sup>, J.L. Sanz<sup>2</sup>, R.B. Barreiro<sup>2</sup> and M. López-Caniego<sup>2</sup>

<sup>1</sup>*Istituto di Scienze e Tecnologie dell’Informazione “A. Faedo”, CNR, via Moruzzi 1, 56124 Pisa, Italy*

<sup>2</sup>*Instituto de Física de Cantabria, avda. Los Castros s/n, 39005 Santander, Spain*

Accepted –. Received –; in original form –

## ABSTRACT

In this work we study the performance of linear multifilters for the estimation of the amplitudes of the thermal and kinematic Sunyaev-Zel’dovich effects. We show that when both effects are present, estimation of these effects with standard matched multifilters is intrinsically biased. This bias is due to the fact that both signals have basically the same spatial profile. We find a new family of multifilters related to the matched multifilters that cancel this systematic bias, hence we call them Unbiased Matched Multifilters. We test the unbiased matched multifilters and compare them with the standard matched multifilters using simulations that reproduce the future Planck mission’s observations. We find that in the case of the standard matched multifilters the systematic bias in the estimation of the kinematic Sunyaev-Zel’dovich effect can be very large, even greater than the statistical error bars. Unbiased matched multifilters cancel effectively this kind of bias. In concordance with other works in the literature, our results indicate that the sensitivity and resolution of Planck will not be enough to give reliable estimations of the kinematic Sunyaev-Zel’dovich of individual clusters. However, since the estimation with the unbiased matched multifilters is not intrinsically biased, it can be possible to use them to statistically study peculiar velocities in large scales using large sets of clusters.

**Key words:** methods: data analysis – techniques: image processing – galaxies: clusters – cosmic microwave background

## 1 INTRODUCTION

The Sunyaev-Zel’dovich effect (Sunyaev & Zel’dovich 1970) is one of the most interesting and promising observational tools for cosmology. During the last four decades, many works have addressed its usefulness as a probe that can be used to determine cosmological parameters (in special when combined with other observational diagnostics such as gravitational lensing or X-ray observations), to study the abundances and evolution of galaxy clusters up to high redshifts, to estimate the gas mass fractions inside clusters, to measure peculiar velocities of the gas and to map the inner structure of galaxy clusters. Some excellent recent reviews on the physics of the SZ effect can be found in Rephaeli (1995) and Birkinshaw (1999). Recent observational results have been reviewed in Birkinshaw (1999) and Carlstrom et al. (2000). Another excellent review that focus in the application of SZ effect observations to cosmology can be found in Carlstrom, Holder & Reese (2002).

While the theory of the SZ effect physics is very well understood, from the observational point of view its study is still difficult. This is mainly due to the faintness of the

effect –specially the elusive kinematic SZ effect– and the presence of many astrophysical “contaminants” in the frequencies where the SZ effect is better observed.

The SZ effect appears as a secondary anisotropy in the Cosmic Microwave Background (CMB), that is, as a small spectral distortion in the CMB spectrum caused by the scattering of CMB photons due to high energy electrons. Therefore, it must be disentangled from the CMB fluctuations themselves, a task that is relatively easy to accomplish in the case of the thermal SZ effect but very difficult in the case of the kinematic SZ. Besides, all the contaminants (or “foregrounds”) that affect CMB observations affect as well SZ effect experiments: extragalactic point sources and Galactic foregrounds such as dust, synchrotron and free-free emissions. As we will show later in this work, even the two different types of SZ effects, the thermal and the kinematic, can be considered as contaminants one of the other.

In the last few years several SZ experiments have reached the sensitivities and angular resolutions needed to, for the first time in history, fully exploit the power of SZ observations. Even more experiments are under construction or planned for the next years (Carlstrom et al. 2000; Carlstrom, Holder & Reese 2002; Aghanim et al. 2004). Ever for these high-sensitivity experiments the observation

\* E-mail: diego.herranz@isti.cnr.it

of the SZ effect is not an easy task, and therefore a great care must be placed in the analysis and interpretation of the data.

Several different approaches lead to the many different SZ data analysis methods proposed in the literature. One approach is the *component separation*, which goal is to extract from the data all the different signals that were present for their separate study. In this context the SZ effect is just one of the products of the separation. Component separation techniques typically make use of the different statistical distribution and spectral behaviour (i.e. the different frequency dependence) of the components. An example of component separation method that has been applied to simulations containing SZ effect is the Maximum Entropy Method, e.g. Hobson et al. (1999). As noted by Diego et al. (2002) and Herranz et al. (2002a), component separation methods can be very powerful but there is a risk when the main goal is to study only one of the sources (in this case the SZ effect): an error in the separation of any one of the components is easily propagated to the others, and therefore it is necessary to be extremely careful that all the assumptions made (such as the frequency dependence of the components, or their statistical independence, etc) are correct.

Another approach focuses only on the one component under study (the SZ in this case), trying to extract it from the data or to estimate a few parameters that characterise it. For example, in the case of the SZ effect we can try to obtain a map of the Compton parameter or just to obtain the positions of the clusters, their integrated fluxes, their peculiar velocities, etc. We will call this approach *detection* and/or *estimation*. Detection/estimation techniques consider all the other components of the data apart from the one under study as interference (noise) and try to minimise its impact. Compared with component separation techniques, they tend to be more robust in the sense that they do not need to model in detail all the different components that form part of the “background”. Examples of this type of techniques applied to SZ data are Bayesian non-parametric mapping of the Compton parameter (Diego et al. 2002), optimal filtering (Haehnelt & Tegmark 1996; Aghanim et al. 1997; Herranz et al. 2002a), Markov Chain Monte Carlo (MCMC) sampling techniques (Hobson & McLachlan 2003) and parameter estimation via simulated annealing (Hansen 2004a).

The choice among the above mentioned techniques is a delicate issue; all of them have some desirable properties and some drawbacks, and depending on the case under study one or another (or even a combination of several of them) will be more appropriate. The good thing is that they are not mutually exclusive and in certain cases they can work together to obtain better results. In general non-linear methods such as MCMC and simulated annealing are more powerful, but they are not free of problems. MCMC methods are expensive and time-demanding from the computational point of view. This make them unpractical for large blind SZ surveys. The SASZ simulated annealing code (Hansen 2004a) is fast but in presence of astrophysical contaminants such as extragalactic point sources and Galactic foregrounds it is likely to suffer from systematic errors that can be relatively large (?).

Linear “optimal” filters may be not so powerful as non-linear detection/estimation techniques, but they have some nice properties that may make us consider their use. They

are simple to understand and implement. They are quite fast and not computationally demanding. Moreover, since they do not need a detailed modelling of the background statistical properties –apart from the fact that it is statistically homogeneous and that it can be properly described by second-order statistics, namely the power spectrum– they are very robust. Moreover, convolutive filters are appropriate to select “compact” features (as clusters of galaxies) in the data by filtering out the large scales where diffuse components manifest and the small scales where pixel noise appear. The multifilters (filters that operate simultaneously on all the frequency channels of an experiment, taking into account the frequency dependence of the SZ effect and the correlations among different channels in order to optimise the detection of the SZ effect) presented in Herranz et al. (2002a) provide a powerful denoising tool (they minimise the background contamination) as well as a straightforward amplitude estimation criterion. In that work two families of multifilters, the matched multifilter (MMF) and the scale-adaptive multifilter (SAMF) were studied and tested on realistic Planck simulations. The results showed that both families of multifilters lead to unbiased estimators of the central value of the Compton parameter of the clusters in the simulations, even in presence of realistic contaminants. MMF give higher gain factors (the ratio between the variance of the background before and after filtering) than the SAMF, keeping the same level of spurious detections, so they are preferred as our tool of choice. The Herranz et al. (2002a) multifilters were designed to detect/estimate the amplitude of the thermal SZ effect. In the same way they can be constructed to detect the more elusive kinematic SZ effect just by changing accordingly the frequency dependence of the effect in the formulae that lead to the expression of the filter.

In the previous discussion we have considered the case when only the thermal (or kinematic) SZ effect is present in the data. But if the two effects appear at the same time, will be the multifilter estimator still unbiased? The answer, as we will see, is no. Multifilters use information on the frequency dependence and the spatial profile of the sources at the same time. If two sources have different frequency dependence and profile they are likely to be separated very well. But if the two sources have the same profile, or the same frequency dependence, the problem will be somewhat degenerated and the estimator will show systematic effects.

A case of two sources with the same frequency dependence but different spatial profile is evident: the kinematic SZ effect and the CMB spectra are identical (except for second-order relativistic effects). This means that some residual contamination from CMB fluctuations will remain after filtering, introducing errors in the estimation of the kinematic SZ. Fortunately, the CMB fluctuations are damped considerably on the angular scales of typical galaxy clusters (see for example Hu & White (1997)). Moreover, since CMB fluctuations can be symmetrically positive or negative, on average the statistical systematic bias due to this effect is zero. Considered individually, however, all kinematic SZ measurements by mean of multifilters will be affected by a non-removable error, and little can be done to solve this problem.

On the other hand, the problem that appears when two signals with the same spatial profile and different frequency dependence are overlapped can be solved. In our case these

two signals are the thermal and the kinematic SZ effects. We will show here that their superposition leads inevitably to systematic errors in the estimation of the SZ parameters when we use standard matched multifilters. These errors can be very large in the case of the kinematic SZ effect and can be very dangerous for automatic blind SZ surveys. This paper is devoted to the study and cancellation of this dangerous type of bias.

The paper is structured as follows. In section 2 we will briefly review the MMF and its properties. In section 3 we will show how the non-removable systematic bias appears in the MMF estimator when two signals with the same spatial profile and location but different frequency dependence are present. Section 4 shows how to design families of multifilters that overcome that problem: the unbiased matched multifilters (UMMF). In section 5 we will test the MMF and the UMMF in realistic Planck simulations. Finally, we will discuss our results in section 6.

## 2 THE STANDARD MATCHED MULTIFILTER

The standard matched multifilter (MMF) was introduced by Herranz et al. (2002a) and, independently, by Naselsky et al. (2002). Following Herranz et al. (2002a), let us consider a set of  $N$  astronomical images corresponding to observations at different frequencies of a given region of the sky. A signal with a known frequency dependence is embedded in the data, so that the observations can be described with the following model:

$$d_\nu(\vec{x}) = f_\nu s_\nu(x) + n_\nu(\vec{x}), \quad \nu = 1, \dots, N. \quad (1)$$

where the *generalised noise*  $n_\nu(\vec{x})$  corresponds to the sum of the other emission components in the map. The background  $n_\nu(\vec{x})$  is modelled as a homogeneous and isotropic random field with average value  $\langle n_\nu(\vec{x}) \rangle = 0$  and cross-power spectrum  $P_{\nu_1\nu_2}(q)$  ( $q \equiv |\vec{q}|$ ) defined by

$$\langle n_{\nu_1}(\vec{q}) n_{\nu_2}^*(\vec{q}') \rangle = P_{\nu_1\nu_2}(q) \delta_D^2(\vec{q} - \vec{q}'), \quad (2)$$

where  $n_\nu(\vec{q})$  is the Fourier transform of  $n_\nu(\vec{x})$  and  $\delta_D^2$  is the 2-D Dirac distribution.

The spatial profile  $s_\nu(x)$  is usually written as the product of the source amplitude  $A$  and a spatial template  $\tau(x)$ . In general, the template at each frequency  $\nu_i$  is the result of the convolution of the normalised profile of the source and the antenna beam at that frequency. Hereinafter, we assume for simplicity that the source has spherical symmetry,  $x \equiv |\vec{x}|$ , but the methods can be generalised for non-symmetric profiles. For simplicity as well we will assume that the source is centred at the position  $x = 0$ .

Equation (1) can be expressed in a more compact way as a vector equation,

$$\mathbf{d}(\vec{x}) = \mathbf{A}\mathbf{F}(x) + \mathbf{n}(\vec{x}). \quad (3)$$

where the elements of vector  $\mathbf{F}$  are  $F_\nu = f_\nu \tau_\nu$ . Hereinafter, we will employ the usual boldface notation for the  $N$ -component vectors in frequency whereas the ‘‘arrow’’ notation  $\vec{x}$ ,  $\vec{q}$  will refer to 2-dimensional vectors in real space or Fourier space.

The goal is to obtain a set of  $N$  linear filters that, once applied to the data, allow us to determine the amplitude  $A$  of the signal with a minimum interference of the contaminant

noise. The filters should take advantage on the knowledge of the frequency dependence of the signal  $\mathbf{f}$ , the characteristic profile of the source  $\tau$  and the cross-power spectrum of the noise, that can be directly estimated from the data. The filters are applied to the  $N$  frequency channels in order to give a quantity –called *filtered map*– at each position that will be used as an estimator of  $A$ . Let  $\Upsilon(\vec{x}) = \{v_{\nu_1}(\vec{x}), \dots, v_{\nu_N}(\vec{x})\}$  the vector of  $N$  filters we are looking for, then the filtered map at the position  $\vec{b}$  is given by

$$w(\vec{b}) = \sum_\nu \int d\vec{x} d_\nu(\vec{x}) v_\nu(|\vec{x} - \vec{b}|), \quad (4)$$

that can be expressed in Fourier space in a very compact way

$$w(\vec{b}) = \int d\vec{q} e^{-i\vec{q}\vec{b}} \mathbf{d}^t(\vec{q}) \Upsilon(q), \quad (5)$$

where the superscript  $t$  denotes vector transposition, and the operation inside the integral is the usual scalar product of vectors. The variance of the filtered map can be expressed as

$$\sigma_w^2 = \langle w^2(\vec{b}) \rangle - \langle w(\vec{b}) \rangle^2 = \int d\vec{q} \Upsilon^t \mathbf{P} \Upsilon. \quad (6)$$

The explicit dependence in  $q$  has been removed from the previous equation for the sake of simplicity of notation. Unless it is necessary to include it, we will do the same in the following.

The MMF is obtained when two constraints are imposed on the filters  $\Upsilon$ :

- (i) That  $w(\vec{0})$  is an *unbiased estimator* of the amplitude of the source, that is,  $w(\vec{0}) = A$ .
- (ii) That  $w(\vec{0})$  is an *efficient estimator* of the amplitude of the source, that is, the variance of the  $w$  values is minimum.

As was shown in Herranz et al. (2002a), the filters that satisfy these conditions are given by:

$$\Upsilon_{MMF} = \alpha^{-1} \mathbf{P}^{-1} \mathbf{F}, \quad \alpha = \int d\vec{q} \mathbf{F}^t \mathbf{P}^{-1} \mathbf{F}, \quad (7)$$

where  $\mathbf{P}^{-1}$  is the inverse matrix of the cross-spectrum  $\mathbf{P}$ . Using eq. (6) we have that for the MMF

$$\sigma_w^2 = \int d\vec{q} \Upsilon_{MMF}^t \mathbf{P} \Upsilon_{MMF} = \alpha^{-1}. \quad (8)$$

## 3 SIGNALS WITH THE SAME SPATIAL PROFILE AND DIFFERENT FREQUENCY DEPENDENCE

The MMF is designed to produce an unbiased and efficient linear estimator of the amplitude of a signal with known frequency dependence and spatial profile in multiwavelength observations. But what happens when there are present two signals with the same spatial profile and location but different frequency dependence? Such is the case, for example, of the thermal and kinetic Sunyaev-Zel’dovich effects. Both effects are superimposed with identical spatial distribution (if we do not take into account intracluster gas motions that can distort the shape of the kinematic effect) but quite different frequency dependence.

### 3.1 Thermal and kinematic Sunyaev-Zel'dovich effects

The thermal SZ effect is due to the inverse Compton scattering of CMB photons by free electrons in the hot intra-cluster gas. It produces a shift in the CMB spectrum to higher frequencies in the direction where the cluster is observed. This effect is characterised by the comptonization parameter  $y_c$ ,

$$y_c = \frac{k_B \sigma_T}{m_e c^2} \int T_e(l) n_e(l) dl, \quad (9)$$

where  $k_B$  is the Boltzmann constant,  $\sigma_T$  the Thomson section,  $m_e$  the electron mass,  $c$  the velocity of light,  $T_e$  and  $n_e$  are the temperature and density of the electrons in the gas and  $l$  is the distance along the line of sight. Ignoring relativistic effects, the frequency dependence of the thermal SZ effect is given by

$$\left(\frac{\Delta T}{T}\right)_{SZt}(\nu) = y_c f(\tilde{\nu}), \quad \tilde{\nu} = \frac{h\nu}{k_B T_{CMB}}, \quad (10)$$

where  $h$  is the Planck constant and  $T_{CMB}$  the temperature of the CMB, and where

$$f(x) = x \frac{e^x + 1}{e^x - 1} - 4. \quad (11)$$

The kinematic SZ effect, on the other hand, is due to the Doppler effect that arises because of the radial peculiar velocity of the cluster  $v_r$  along the line of sight. The intensity of the kinematic effect, not taking into account second-order relativistic corrections and considering  $T_e$  to be constant along the cluster, is

$$\left(\frac{\Delta T}{T}\right)_{SZk}(\nu) = -y_c \frac{v_r m_e c}{k_B T_e}, \quad (12)$$

and the frequency dependence is (again ignoring relativistic corrections) constant in  $\Delta T/T$  units. The intensity of the kinematic effect is in general significantly smaller than the intensity of the thermal effect.

At high frequencies, the expressions given above are not accurate and relativistic corrections should be taken into account when dealing with real data. In this work we restrict the discussion to the non-relativistic case for simplicity.

### 3.2 Bias in the MMF estimator

Combining the two SZ effects our data model is

$$\mathbf{d}(\vec{x}) = \left(\frac{\Delta T}{T}\right)_{SZt+k} = y_c [\mathbf{F}(\vec{x}) - V\tau(\vec{x})] + \mathbf{n}(\vec{x}), \quad (13)$$

where  $V = (v_r m_e c)/(k_B T_e)$  and the vector  $\mathbf{F}$  is constructed using the profile  $\tau$  and the thermal SZ frequency dependence in eqs. (10) and (11).

Imagine a MMF designed for the detection of the thermal SZ effect is applied to the data in (13). The filter will be the one given in eq. (7) using the vector  $\mathbf{F}$  that corresponds to eq. (13). It is easy to calculate the average value of the filtered map:

$$\begin{aligned} \langle w_t(\vec{0}) \rangle &= \int d\vec{q} y_c [\mathbf{F}^t - V\tau^t] \Upsilon_{MMFt} = \\ y_c \alpha^{-1} \int d\vec{q} \mathbf{F}^t \mathbf{P}^{-1} \mathbf{F} - y_c V \alpha^{-1} \int d\vec{q} \tau^t \mathbf{P}^{-1} \mathbf{F} = \\ & y_c - y_c V \frac{\beta}{\alpha}, \end{aligned} \quad (14)$$

where the constant  $\beta$  is defined as

$$\beta = \int d\vec{q} \tau^t \mathbf{P}^{-1} \mathbf{F}. \quad (15)$$

According with eq. (14), due to the presence of the kinematic SZ effect the estimator  $w_t(\vec{0})$  is not longer unbiased, and the estimation of  $y_c$  will have a systematic error proportional to  $V\beta/\alpha$ .

The same will occur when a MMF designed for the detection of the kinematic SZ effect. In that case, the frequency dependence to be used is a constant whose value can be included in  $V$  and therefore  $f_\nu = 1$ . The shape of the MMF is then

$$\Upsilon_{MMFk} = \gamma^{-1} \mathbf{P}^{-1} \tau, \quad \gamma = \int d\vec{q} \tau^t \mathbf{P}^{-1} \tau, \quad (16)$$

The average value of the filtered map is then

$$\begin{aligned} \langle w_k(\vec{0}) \rangle &= \int d\vec{q} y_c [\mathbf{F}^t - V\tau^t] \Upsilon_{MMFk} = \\ y_c \gamma^{-1} \int d\vec{q} \mathbf{F}^t \mathbf{P}^{-1} \tau - y_c V \gamma^{-1} \int d\vec{q} \tau^t \mathbf{P}^{-1} \tau = \\ & y_c \frac{\beta}{\gamma} - y_c V. \end{aligned} \quad (17)$$

Note that since  $y_c$  and  $V$  appear as a product in eq. (13),  $\langle w_k(\vec{0}) \rangle$  is not a direct estimator of  $V$  but of the quantity  $y_c V$ . Dividing by  $y_c$  and changing the signs we obtain

$$-\frac{\langle w_k(\vec{0}) \rangle}{y_c} = V - \frac{\beta}{\gamma}, \quad (18)$$

and therefore we find that our estimator is again biased.

As we will see later in section 5, in the case of microwave observations of the SZ effect, the bias in the MMF estimator of the thermal SZ effect is normally negligible, but in the case of the kinematic SZ effect it is expected to be very large, of the order of the effect itself or even bigger. Therefore, this bias must be taken into account and corrected.

### 3.3 Cancelling the bias

There are several ways in which the bias described above can be taken into account. The first option is simply to separate the thermal and kinematic effects before estimating their amplitudes. This goal can be attained using a convenient component separation technique, for example the Maximum Entropy Method (Hobson et al. 1999), non-parametric Bayesian detection (Diego et al. 2002) or MCMC sampling techniques (Hobson & McLachlan 2003). The problem is that in practise no component separation technique works perfectly, and some uncontrolled residuals always remain that will still bias the estimation of the amplitude of the effects.

A second option consists in using eqs. (14) and (18) to subtract the bias factor in each case. This is a perfectly licit option in principle, but can be a little difficult to carry out in a real case. The argument is as follows: to determine the bias in  $y_c$  we need, according to eq. (14), to know the value of  $y_c V$ , whose estimation is biased. To remove the bias in  $y_c V$  we need, according to eq. (18), to know the value of  $y_c$ , which is biased as well. Moreover, on an individual basis (cluster by cluster) the quantities  $V$  and  $y_c$  will be estimated

with a non-zero error. Therefore, trying to cancel the bias in this way leads us to a vicious circle. In section 5 we will see that for the case of the future Planck satellite observations the bias in  $y_c$  will be small, and the vicious circle could be circumvented just by considering the estimated  $y_c$  as the correct one. This would however introduce further errors in any case. Besides, in other experiments the bias in  $y_c$  can be not so small as in the Planck case is. Therefore, we do not recommend this option to cancel the bias of the MMF. In the next section we will describe two novel lineal multifilters that automatically cancel the bias in the estimation of the thermal and kinematic SZ amplitudes.

#### 4 UNBIASED MATCHED MULTIFILTER

Instead of following any of the approaches described in section 3.3, let us see if it is possible to design linear filters that are nearly as efficient as the MMF and do not show the systematic bias described above. To do it we will make use of the knowledge on the two distinct frequency dependences of the thermal and kinematic SZ effects. The resulting filters will be called *unbiased matched multifilters* (UMMF). Specifically, we search for a set of filters specifically designed to give the thermal amplitude  $y_c$  without bias and a different set of filters specifically designed to give the kinematic amplitude  $y_c V$ .

##### 4.1 Unbiased Matched Filter for the thermal SZ effect

We construct the filters  $\Psi = \{\psi_{\nu_1}, \dots, \psi_{\nu_N}\}$  so that the filtered map  $w_\Psi$  satisfies the canonical matched filter conditions plus another one aimed at cancelling the bias due to the presence of the kinematic effect.

(i) The filters, when applied to the thermal part of eq. (13), give, at the position of the source, the value of the comptonization parameter, that is,

$$\int d\vec{q} \mathbf{F}^t \Psi = 1, \quad (19)$$

(ii) The filters, when applied to the kinematic part of eq. (13), give, at the position of the source, no contribution to the filtered map, that is,

$$\int d\vec{q} \tau^t \Psi = 0, \quad (20)$$

(iii) The variance of the filtered map,  $\sigma_{w_\Psi}$ , is minimum (*efficient* estimator).

The two first two conditions ensure that the filtered map at the position of the source is an unbiased estimator of the thermal SZ effect. The third one is the condition for efficiency of the estimator. The filters that satisfy the previous three conditions are

$$\Psi = \frac{1}{\Delta} \mathbf{P}^{-1} (\gamma \mathbf{F} - \beta \tau), \quad \Delta = \alpha \gamma - \beta^2, \quad (21)$$

where the constants  $\alpha$ ,  $\beta$  and  $\gamma$  are defined in equations (7), (15) and (16). It is straightforward to see that  $\langle w_\Psi(\vec{0}) \rangle = y_c$  and that the variance of the filtered map is

$$\sigma_{w_\Psi}^2 = \frac{\gamma}{\Delta}. \quad (22)$$

##### 4.2 Unbiased Matched Filter for the kinematic SZ effect

Let us now find the filters  $\Phi = \{\phi_{\nu_1}, \dots, \phi_{\nu_N}\}$  so that the filtered map  $w_\Phi$  satisfies the canonical matched filter conditions plus another one aimed at cancelling the bias due to the presence of the thermal effect.

(i) The filters, when applied to the thermal part of eq. (13), give, at the position of the source, no contribution to the filtered map, that is,

$$\int d\vec{q} \mathbf{F}^t \Phi = 0, \quad (23)$$

(ii) The filters, when applied to the kinematic part of eq. (13), give, at the position of the source, the value of the product  $y_c V$ , that is,

$$\int d\vec{q} \tau^t \Phi = 1, \quad (24)$$

(iii) The variance of the filtered map,  $\sigma_{w_\Phi}$ , is minimum (*efficient* estimator).

The two first two conditions ensure that the filtered map at the position of the source is an unbiased estimator of the kinematic SZ effect. The third one is the condition for efficiency of the estimator. The filters that satisfy the previous three conditions are

$$\Phi = \frac{1}{\Delta} \mathbf{P}^{-1} (-\beta \mathbf{F} + \alpha \tau), \quad (25)$$

where the constants  $\alpha$ ,  $\beta$ ,  $\gamma$  and  $\Delta$  are the same as in eq. (21). It is straightforward to see that  $\langle w_\Phi(\vec{0}) \rangle = y_c V$  and that the variance of the filtered map is

$$\sigma_{w_\Phi}^2 = \frac{\alpha}{\Delta}. \quad (26)$$

## 5 APPLICATION TO SIMULATED PLANCK DATA

As a test of the previous ideas, we now apply both the standard and the unbiased matched multifilters to simulated Planck observations in order to estimate the thermal and kinematic SZ of test clusters placed on the simulations. Our goal is just to show by an example how the biases described in section 3 appear and how the unbiased matched multifilters are able to cancel it. Therefore, to keep the example simple and clear we will restrict ourselves to ideal conditions in which the spatial profile of the clusters is perfectly known from the beginning. A full study of the performance of the filters in the Planck case, including uncertainties in the cluster profile, asymmetric profiles and realistic cluster distributions is out of the scope of this work and will be addressed in the future.

We will focus specially on filters designed to extract the kinematic SZ effect. Note that due to the extreme faintness of the kinematic SZ effect the task of detecting it is going to be very difficult. In fact, Planck sensitivities, angular resolution and noise levels do not make it the best experiment to study the kinematic SZ effect. In spite of this, we choose the Planck mission as our example scenario for two reasons. The first one is that Planck's instrumental specifications, noise levels and performance have been thoroughly

**Table 1.** Technical characteristics of the 9 simulated Planck channels. Column two lists the FWHM assuming a Gaussian beam. Column three shows the pixel size in arcmin adopted in our simulations. In column four the instrumental noise variance per pixel is given in  $\Delta T/T$  units (thermodynamic temperature).

Frequency (GHz)	FWHM (arcmin)	Pixel size (arcmin)	$\sigma_{noise}$ ( $\Delta T/T$ )
30	33.0	6.0	$1.1 \times 10^{-5}$
44	24.0	6.0	$1.1 \times 10^{-5}$
70	13.0	3.0	$2.2 \times 10^{-5}$
100	9.2	3.0	$6.1 \times 10^{-6}$
143	7.1	1.5	$1.0 \times 10^{-5}$
217	5.5	1.5	$1.6 \times 10^{-5}$
353	5.0	1.5	$4.9 \times 10^{-5}$
545	5.0	1.5	$4.9 \times 10^{-4}$
857	5.0	1.5	$2.2 \times 10^{-2}$

studied in the literature, and realistic simulations of Planck observations are relatively easy to produce and analyse. The second reason is that at Planck’s angular resolution most of the clusters will appear as point sources in the sky. Therefore, their observed profile will be practically equal to the well-known beam profile of the Planck detectors. Then, the assumption that the spatial profile of the clusters is known is not so unreasonable.

## 5.1 Simulations

Even though for this work we are going to use very simplistic toy clusters and non-relativistic SZ effects, we intend to simulate the other astrophysical and instrumental signals that constitute the generalised noise  $\mathbf{n}(\vec{x})$  in eq. (3) in the most realistic way possible. Our simulations include the latest available information about the physical components of the emission (CMB, Galactic foregrounds and extragalactic point sources) and the technical specifications of the different Planck channels. The simulations were performed in patches of the sky of  $12.8^\circ \times 12.8^\circ$ . Table 1 shows the assumed observational characteristics of the simulated maps.

The  $C_\ell$ ’s for the CMB simulation were generated using the CMBFAST code (Seljak & Zaldarriaga 1996) for a spatially-flat  $\Lambda$ CDM Universe with  $\Omega_m = 0.3$  and  $\Omega_\Lambda = 0.7$  (Gaussian realisation). The simulated Galactic emission includes four components: thermal dust, spinning dust, free-free and synchrotron. The details of the Galactic foreground simulations are identical to those described in Herranz et al. (2002a) (see references therein). The extragalactic point source simulations come from the model of Toffolatti et al. (1998) for a Gaussian realisation with the same cosmological parameters used for the CMB simulation.

Synthetic clusters were simulated using the spatial profile

$$\tau(x) = \frac{r_c r_v}{r_c + r_v} \left( \frac{1}{\sqrt{r_c^2 + x^2}} - \frac{1}{\sqrt{r_v^2 + x^2}} \right). \quad (27)$$

The previous profile is a modification of the basic multi-quadric profile in which  $r_c$  takes the role of the core radius of the cluster and  $r_v$  is a limiting cut scale that can be associated with the virial radius of the clusters. For  $x \ll r_v$

the profile in eq. (27) behaves like the classical  $\beta$  model (with  $\beta = 1/2$ ) whereas for  $x \gg r_v$  the profile quickly drops to zero. The profile in eq. (27) is continuous, gives a good approximation for the typical cluster profile and is well-behaved in Fourier space. For this work we used  $r_v = 10r_c$ .

## 5.2 Preliminary analysis of the simulations

Given a set of maps corresponding to the simulations described above for the nine Planck frequencies, it is easy to estimate the values of the cross-power matrix  $\mathbf{P}$  and therefore to calculate the values of integrals  $\alpha$ ,  $\beta$  and  $\gamma$  for this case. Doing so, we obtain the values

$$\begin{aligned} \alpha &= 2.3721 \times 10^{10} \\ \beta &= -1.4482 \times 10^9 \\ \gamma &= 1.3694 \times 10^9 \\ \Delta &= 3.0386 \times 10^{19}. \end{aligned} \quad (28)$$

According to these numbers and eqs. (22) and (26) we should expect that after using the filters  $\Psi$  and  $\Phi$  the filtered maps should have variances  $\sigma_\Psi \simeq 6.7 \times 10^{-6}$  and  $\sigma_\Phi \simeq 2.8 \times 10^{-5}$ , in  $\Delta T/T$  units.

Let us remember that for the case of the classical matched multifilters the expected variances of the filtered maps should be  $\sigma_{MMFt} = (1/\alpha)^{1/2} \simeq 6.5 \times 10^{-6}$  and  $\sigma_{MMFk} = (1/\gamma)^{1/2} \simeq 2.7 \times 10^{-5}$ , respectively. Then the addition of the bias cancellation constraint in the formulation of the UMMF leads to a small increment of the variance of the filtered maps, but a very small one indeed.

On the other hand, from equations (14) and (18) it is possible to calculate the expected biases that will arise with the standard MMF. Let us denote the estimation of a quantity  $\xi$  with the standard MMF as  $\hat{\xi}$ . We have for the case of the Planck simulations that

$$\begin{aligned} \frac{\hat{y}_c}{y_c} &= 1 + 0.06V, \\ \frac{\hat{V}}{V} &= 1 + \frac{1.05}{V}. \end{aligned} \quad (29)$$

Depending on the value of  $V$ , some of the previous quantities can be considerable. Typical values are  $V \leq 0.1$ , and therefore we find that for the case of the thermal effect the bias will be negligible ( $\hat{y}_c/y_c \simeq 1$ ) whereas for the kinematic effect the bias is huge ( $\hat{V}/V \simeq 10$ ) and can not be discarded. *Standard MMF for the estimation of the kinematic SZ effect is strongly biased.*

The expected errors in the estimation of the amplitudes of the thermal and kinematic effects by means of the multifilters is directly related to the variances of the filtered map calculated above. Note that in the case of Planck the variances in the maps filtered with “kinematic-type” multifilters (both  $\Phi$  filters and MMFk) are higher than the variances for the “thermal-type” multifilters. That is bad news. It implies that the detection and estimation of the kinematic effect by means of multifilters is difficult not only due to the faintness of the effect, but also to the relatively high intrinsic variance of the filtered map.

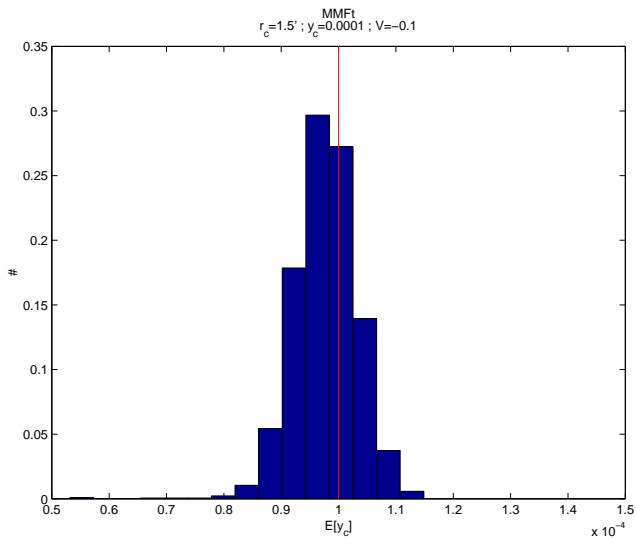


**Figure 1.** Normalised histogram of the values of the estimated  $y_c$  parameter using standard MMFt for the thermal SZ effect. The true value of  $y_c$  is shown with a vertical red line.

### 5.3 Test

In order to test whether the numbers obtained above are correct or not we ran a set of simulations, including synthetic clusters with the profile (27) and the frequency law (13). We simulated 5000 of these clusters. In order to avoid cluster overlapping only five cluster per simulated sky map were included. For this test, we simulated very bright and big clusters, with fixed parameters  $r_c = 1.5$  arcmin,  $y_c = 10^{-4}$  and  $V = -0.1$ . For a temperature of the electrons  $T_e \simeq 5$  keV that value of  $V$  corresponds to a velocity along the line of sight of  $v_r \simeq 300$  kms $^{-1}$ . The simulations were filtered with standard matched multifilters designed for the detection/estimation of both thermal and kinematic SZ effects as well as with the  $\Psi$  and  $\Phi$  unbiased matched multifilters.

We will focus here in the performance of the filters regarding the *estimation* of the SZ effects. We will assume that the presence of the clusters is already established and their locations well known. We would like to remark that in a more general situation, where detection must be achieved before estimating the parameters, other sources of systematic bias different from the one discussed in this work may arise due to the detection criterion itself. For example, if detection is done by looking for local maxima in the images, clusters located in areas where the background is positive will be favoured for detection, and then in the background will not have zero mean *in the areas where clusters are detected*, leading to a new source of bias. For a more complete discussion on this, see for example Herranz et al. (2002b) and López-Caniego et al. (2004). These bias depend on the choice of the detection device and their study is out of the scope of this work.

#### 5.3.1 Performance of MMFt

Figure 1 shows the results of the estimation of  $y_c$  for the 5000 simulated clusters using the standard MMFt for the thermal SZ effect. The average value of the estimated  $y_c$  is  $\langle \hat{y}_c \rangle = 9.77 \times 10^{-5}$  and the dispersion around this value is

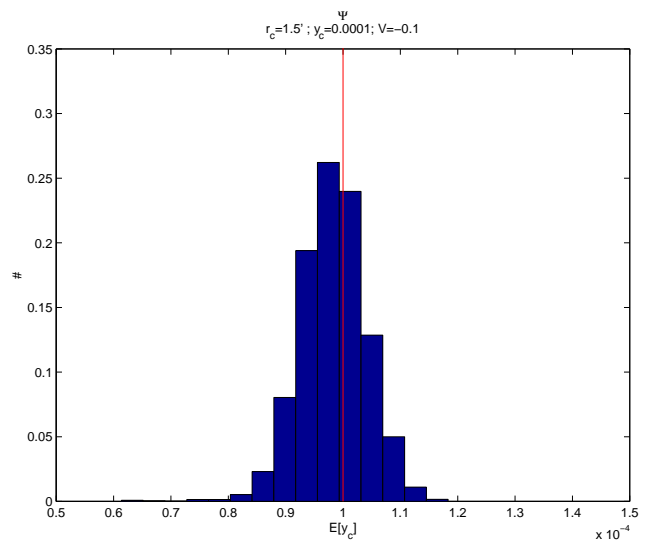


**Figure 2.** Normalised histogram of the values of the estimated  $y_c$  parameter using  $\Psi$  UMMF for the thermal SZ effect. The true value of  $y_c$  is shown with a vertical red line.

$\sigma_{y_c} = 5.4 \times 10^{-6}$ . The average standard deviation of the filtered maps is, for comparison,  $\sigma_{w_{MMFt}} = 6.2 \times 10^{-6}$ . The value for this quantity that was predicted in section 5.2 was  $6.5 \times 10^{-6}$ . Eq. (29) predicts  $\hat{y}_c/y_c = 0.994$ , and the value that is found in the simulations is  $\hat{y}_c/y_c = 0.977$ .

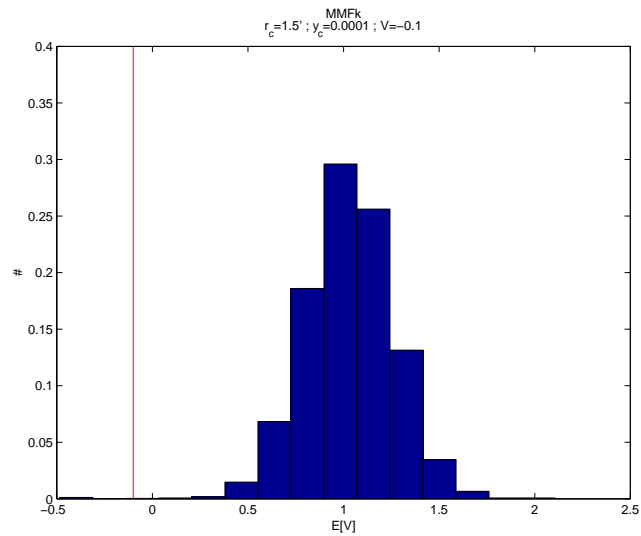
#### 5.3.2 Performance of Psi multifilters

Figure 2 shows the results of the estimation of  $y_c$  for the 5000 simulated clusters using the unbiased  $\Psi$  multifilters for the thermal SZ effect. The average value of the estimated  $y_c$  is  $\langle \hat{y}_c \rangle = 9.83 \times 10^{-5}$  and the dispersion around this value is  $\sigma_{y_c} = 5.7 \times 10^{-6}$ . The average standard deviation of the filtered maps is, for comparison,  $\sigma_{w_\Psi} = 6.5 \times 10^{-6}$ . The value for this quantity that was predicted in section 5.2 was  $6.7 \times 10^{-6}$ . A small bias is present as well in this case, that can be attributed to the finite size of the sample. Hence, for this case both the  $\Psi$  and the standard MMFt multifilters perform similarly well, down to the precision of the simulations.

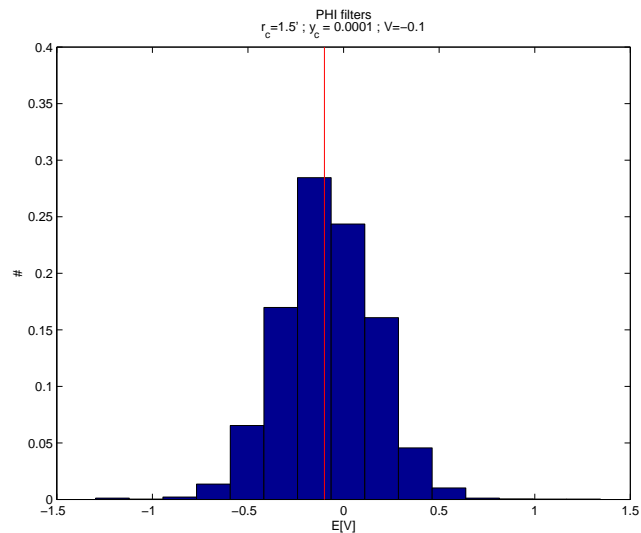
#### 5.3.3 Performance of MMFk

Figure 3 shows the results of the estimation of  $V$  for the 5000 simulated clusters using the standard MMFt for the kinematic SZ effect. The average value of the estimated  $V$  is  $\langle \hat{V} \rangle = 1.05$  and the dispersion around this value is  $\sigma_V = 0.24$ . The average standard deviation of the filtered maps is, for comparison,  $\sigma_{w_{MMFk}}/y_c = 0.236$ . The value for this quantity that was predicted in section 5.2 was 0.27. Eq. (29) predicts  $\hat{V}/V = -9.5$ , and the value that is found in the simulations is  $\hat{V}/V = -10.5$ .

The previous results have been obtained without previous knowledge of  $y_c$ , that is, the estimation of  $V$  for each simulated cluster is obtained by dividing the filtered map at the position of the cluster by the value  $\hat{y}_c$  estimated with the MMFt. Therefore, the errors in the estimation of  $y_c$  do propagate and affect the estimation of  $V$ . If we assume that  $y_c$  is perfectly known we can use its nominal value ( $y_c = 0.0001$



**Figure 3.** Normalised histogram of the values of the estimated  $V$  parameter using standard MMF for the kinematic SZ effect. The true value of  $V$  is shown with a vertical red line.



**Figure 4.** Normalised histogram of the values of the estimated  $V$  parameter using  $\Phi$  multifilters for the kinematic SZ effect. The true value of  $V$  is shown with a vertical red line.

in this case) and then we obtain  $\langle \hat{V} \rangle = 1.03$  and  $\sigma_V = 0.23$ . We conclude that the uncertainty on  $y_c$  is relatively unimportant in this case.

### 5.3.4 Performance of $\Phi$ multifilters

Figure 4 shows the results of the estimation of  $V$  for the 5000 simulated clusters using the  $\Phi$  multifilters for the kinematic SZ effect. The average value of the estimated  $V$  is  $\langle \hat{V} \rangle = -0.08$  and the dispersion around this value is  $\sigma_V = 0.26$ . The average standard deviation of the filtered maps is, for comparison,  $\sigma_{w_\Phi}/y_c = 0.249$ . The value for this quantity that was predicted in section 5.2 was 0.28. The bias has been very much reduced, and the small deviation from zero

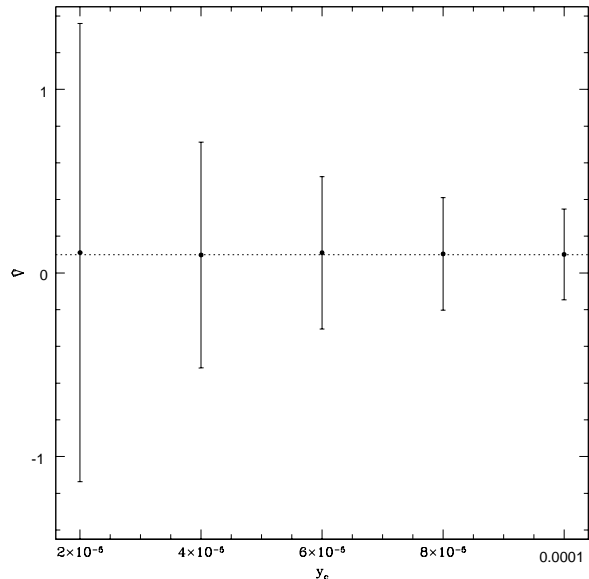


**Figure 5.** Estimation of the  $V$  parameter using  $\Phi$  multifilters for different values of the comptonization  $y_c$ . The true value is indicated with an horizontal dotted line.

can in our opinion be attributed to the limited size of the sample and the large variance of the filtered maps.

If we assume that  $y_c$  is perfectly known we can use its nominal value ( $y_c = 0.0001$  in this case) and then we obtain  $\langle \hat{V} \rangle = -0.08$  and  $\sigma_V = 0.25$ . We conclude that the uncertainty on  $y_c$  is relatively unimportant in this case as well.

### 5.4 Further tests on the $\Phi$ multifilters

The toy clusters used above have large values of the comptonization  $y_c$  and the peculiar velocity. Only a few clusters in the sky are expected to have such large values of these parameters at the same time. Though they serve well for our academic test, it is necessary to determine if the filters are still unbiased in more realistic cases where the cluster parameters take lower values. We performed two sets of simulations varying the value of  $y_c$  and  $V$ . The same as before, for each value of  $y_c$  and  $V$  we simulated 5000 clusters, only five of them per map. The core radius was fixed to  $r_c = 1$  pixel.

Figure 5 shows how the  $V$  parameter is estimated when varying the comptonization  $y_c$ . The true value of the velocity parameter was fixed to  $V = 0.1$ . The estimation is unbiased even for low values of  $y_c$ . The error bars grow as  $y_c$  decreases, which is not unexpected since  $\sigma_V = \sigma_{w_\Phi}/y_c$ .

Figure 6 shows how the  $V$  parameter is estimated when fixing  $y_c = 10^{-4}$  and changing the velocity of the cluster. The velocity can be positive or negative. The estimation is unbiased for all the considered cases, even for the case  $V = 0$ .

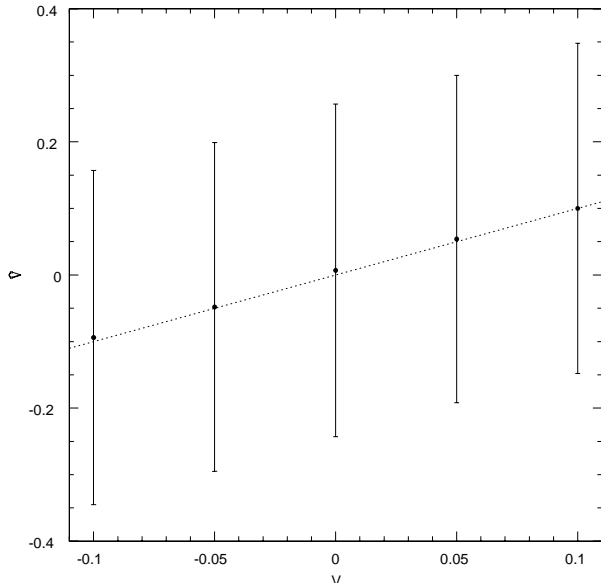


**Figure 6.** Estimation of the  $V$  parameter using  $\Phi$  multifilters for different values of the true value of  $V$ . The true value is indicated with a dotted line.

## 6 DISCUSSION

In this work we have studied the performance of multifilters used to enhance the Sunyaev-Zel’dovich effect signal in CMB maps such as the future Planck satellite will obtain. The aim of multifilters is to boost the cluster signal with respect to the background (CMB plus other astrophysical sources plus noise) so that they can be more easily detected and studied. Multifilters can be used alone or as a previous step before more sophisticated data analysis tools are applied to extract the maximum possible amount of information from the data.

A problem arises when two different signals with different frequency dependence but the same spatial profile appear in a given position. Such is the case of the thermal and kinematic SZ effects. In that case, we have shown that standard matched multifilters are intrinsically biased. This bias can be very strong in the case of the weak kinematic SZ effect. We have designed a family of unbiased matched multifilters that cancelate this bias. The price paid for this bias cancellation is a small decrease on the gain factor with respect to the standard matched multifilters. Unbiased matched multifilters use the *a priori* knowledge on both thermal and kinematic SZ effect’s frequency dependences simultaneously in order to optimise the accuracy of the estimation. We have tested the performance of both standard and unbiased matched multifilters using realistic simulations of the nine Planck’s frequencies. The simulations contain CMB, the main Galactic foregrounds, extragalactic point sources and instrumental noise with the levels expected for the different Planck channels. With these simulations we have shown that standard matched multifilters can estimate the kinematic SZ effect with systematic biases much larger than the true value of the effect. This problem is automatically solved using unbiased matched multifilters. The results

of the numerical tests agree very well with the theoretical expectations.

Our tests show that the statistical error bars in the determination of the cluster parameters  $y_c$  and  $V$  (or, equivalently, the cluster velocity  $v_r$ ) are directly related to the standard deviation of the filtered map; in the case of the thermal SZ effect this last quantity does not depend on the intensity of the SZ effect but on the properties of the background (i.e. the cross-power spectrum matrix) and the shape of the filter (given by the source and beam profiles). For the Planck sky patches here considered and using  $\Psi$  multifilters, the typical error bars in the determination of  $y_c$  are  $\sigma_{y_c} \sim 6 \times 10^{-6}$ , independently of the value of the comptonization of the clusters, which means that for “bright” clusters ( $y_c \sim 10^{-4}$ ) individual comptonizations can be determined with errors  $\sim 20\%$  using the Planck satellite and linear multifilters. In the case of the kinematic SZ effect, to obtain  $V$  ( $v_r$ ) it is necessary to divide the filtered map by  $y_c$ , so error bars are larger for low comptonizations (as reflected by figure 5). For clusters as considered here, with  $y_c = 10^{-4}$  and temperature  $T_e \simeq 5$  keV, the  $\Phi$  multifilters give statistical error bars  $\sigma_V \simeq 0.26$ , that is,  $\sigma_{v_r} \simeq 800$  km  $s^{-1}$ . The situation becomes worse for fainter clusters. This means that Planck will not be able to tell us the velocities of individual clusters<sup>1</sup>. Since  $\Phi$  multifilters provide an unbiased estimator of the kinematic SZ effect it may be possible, however, to determine mean peculiar velocities on large scales by averaging over many clusters. On the other hand, standard matched multifilters would lead to erroneous estimations of mean peculiar velocities due to their intrinsic bias.

One of the strongest traits of linear filtering is that it requires only a small number of assumptions about the data to work. The multifilters need only three information elements to do their work: the frequency dependence of the SZ effects, a reasonable knowledge on the generic cluster profile (and the instrumental beam at each frequency) and the cross-power spectra of the different channels’ background. Uncertainties and errors in the *a priori* information must be kept to a minimum and, when present, they should be taken into account. In the following we will discuss briefly some of the expected problematics that will arise in real life clusters, and suggest a few ways to deal with them.

### 6.1 SZ frequency dependence

The frequency dependence of the thermal and the kinematic SZ effects are very well known, so few surprises will come from this direction. Second-order relativistic corrections, however, can play a role, changing the spectral shape of the effects. In particular, relativistic effects can change the crossover frequency of the thermal SZ effect, a region that is fundamental to the detection of the kinematic SZ effect. The sensitivity of Planck will be too low to constrain the optical depth of relativistic electrons  $\tau_{rel}$  of individual clusters (Enßlin & Hansen 2004). For other more sensitive

<sup>1</sup> At least if only multifilters are used to estimate the kinematic SZ effect. Maybe the combination of the multifiltering technique – as a denoising step – with more sophisticated estimation methods already suggested in the literature could help to improve these results. This is an exciting open possibility for future work.

experiments it may be necessary to take this effect into account. The relativistic correction to the thermal SZ effect frequency dependence is given by Rephaeli (1995) and it is a function of the frequency  $\nu$  and the temperature of the electrons in the intracluster gas  $T_e$ . The relativistic correction to the kinematic SZ effect is due to the Lorentz boost to the electrons caused by the bulk velocity, introduces very small spectral distortions on the kinematic SZ frequency dependence and for a 10 keV cluster moving at 1000 km s<sup>-1</sup> the effect is about an 8 % of the non-relativistic term. If  $T_e$  is known, the relativistic corrections can be calculated, eqs. (10) and (12) can be correspondingly modified and the method can be used without problems.

If  $T_e$  is not known, it can be considered as another quantity to be estimated. In principle, multifilters such as these here described are able to estimate only amplitudes. However, Herranz et al. (2002b) showed a way to estimate additional parameters by means of consecutive linear filterings. In that work, the additional parameter to be estimated was the core radius (as we will discuss later) and the filter under study was the scale-adaptive filter. It is straightforward to generalise the idea to UMMF and other parameters such as the frequency dependence. The philosophy of the method is as follows: it can be shown that matched filters (an unbiased matched filters) give a maximum amplification of the sources when the correlation between the shape of the filter and the shape of the source is perfect. If for example the shape (profile) of the source is known except for a scale factor (such as the core radius), we can filter the image with a number of different matched filters with varying core radius parameter, and study how amplification changes with  $r_c$ . The value of the test parameter at which the maximum amplification is obtained will be our estimate of  $r_c$ . The same applies to multifilters: the maximum amplification will be obtained when the frequency dependence assumed for the filter matches the true one. Then, we can pass a set of different multifilters with varying frequency dependences (in this case, parametrised by different values of  $T_e$ ). The maximum amplification occurs when the value of  $T_e$  of the multifilter coincides with the true one.

## 6.2 Cluster profiles

For the sake of clarity we have deliberately kept the examples presented here as very simple, academic tests, at least regarding to our SZ cluster simulations. On the other hand, the background simulations –CMB, Galactic foregrounds, extragalactic point sources and Planck instrumental noise levels as well as pixel and beam sizes– are very realistic. The purpose of this is to focus on the effect of the “contaminants” rather than the whole problem. Unfortunately, in real life clusters are not so nicely symmetric and we do not have a perfect *a priori* knowledge of their spatial profile. Luckily, we neither have a total ignorance about it. Normally we have some previous idea about how clusters look like. The main uncertainties here are:

### 6.2.1 Size uncertainties

Clusters of many different sizes do appear in CMB maps. Throughout the examples presented in this work we assumed

that all the clusters had the same core radius  $r_c$ , which was known a priori. Herranz et al. (2002b) provided a method to deal with this uncertainty using the scale-adaptive filter on a single map. The generalization to multifilters is straightforward (Herranz et al. 2002a). The basic idea is to filter the maps with a set of different filters varying the  $r_c$  parameter and then to look for the maximum gain cluster by cluster. With this method it is possible to determine the value of  $r_c$  with typical errors lower than the pixel size (Herranz et al. 2002b).

### 6.2.2 Profile shape

If instead of the modified multiquadric profile used in eq. (27) the cluster has a different profile the matching between the filter and the cluster will not be perfect and the filtering will loose performance. This will be an important issue in high resolution experiments where the cluster size is much larger than the beam size. In the case of Planck most clusters will be smaller than the beam size and after convolution their observed shapes will be dominated by the beam profile. Therefore, in the case of Planck the errors due to profile uncertainties will be small except for a few cases of very extense clusters.

For these few extense cluster and for the case of high resolution experiments we suggest the use of an iterative technique to adaptively fit the true profile of a cluster in an empiric way. Starting with a given profile guess such as the one in eq. (27), the shape of the profile can be slowly varied in successive steps, introducing small filter shape perturbations and maximising the signal to noise gain after filtering. The maximum gain corresponds to the best fit between the profile of the filter and the profile of the cluster. A method for adaptive shape fitting that could be adapted to this problem has been successfully accomplished in the modelling of gravitational lensing effect due to massive galaxy clusters (see for example Broadhurst et al. (2004)). We will explore this possibility in a future work.

### 6.2.3 Non-circular profiles

In this work we have assumed symmetric circular profiles and beams. This condition can be relaxed without loss of generality. If the non-symmetric profile is previously known (for example thanks to high-resolution observations in X-ray or other wavelengths) specific non-symmetric filters can be calculated without problem. If the shape of the cluster is not previously known, an iterative scheme such as the previously mentioned can be attempted.

### 6.2.4 Non iso-thermal clusters

It is frequent to consider that  $T_e$  is constant all along the cluster, which allows us to write nicely the kinematic SZ effect as in eq. (12). But galaxy clusters are not iso-thermal. As a consequence of this, cluster parameters derived through the observation of SZ effect will be affected. Hansen (2004b) has shown that peculiar velocities will be systematically shifted by 10 – 20% if the inner structure of the cluster is

not considered in detail, which requires either observationally expensive X-ray observations or high angular resolution SZ observations.

### 6.3 Background power spectrum

The background power spectrum can usually be estimated directly from the data. This is a safe practise if SZ clusters' contribution to the total power spectrum is relatively small. Such is the case expected for the Planck mission. If the SZ clusters were so strong that they contributed significantly to the total power spectrum at all the scales, they would be so conspicuous that detection would not be a problem, and multifiltering would not be necessary.

### 6.4 Extragalactic point source contamination

Historically, extragalactic point sources have been the strongest source of contamination in SZ observations. In this work we have included realistic point source simulations using the Toffolatti et al. (1998) model, whose predictions for the radio source counts have been recently confirmed by the WMAP mission (Bennett et al. 2003). We have shown that multifilter estimation is not substantially affected by these point sources. There are however two details that have not been included in the simulations and can affect the estimation of cluster parameters: the intrinsic galaxy clustering and the spatial correlation between individual galaxies and galaxy clusters.

#### 6.4.1 Point source clustering

We used the point sources of the Toffolatti et al. (1998) model assuming a uniform Poisson distribution of galaxies in the sky. In the real sky, however, galaxies are spatially correlated due to clustering. Temperature fluctuations due to unresolved point sources are stronger if clustering is considered. Apart from increasing the error bars, Aghanim et al. (2004) have shown that this effect leads to significant systematic errors in the determination of the thermal and kinematic SZ amplitudes by means of the SASZ method (Hansen 2004a). It is not clear how galaxy clustering will affect the multifiltering method presented in this work. If the correlation scale of the galaxies is similar to the cluster size systematic shifts can occur<sup>2</sup>, but if the unresolved galaxies' fluctuation field is not correlated with the positions of the clusters the effect should be small. This is a problem worth to study in future works.

#### 6.4.2 Point sources associated to clusters

Another factor not considered in the simulations is the associations between clusters and individual galaxies. These associations can be due to the galaxies that form part of the

cluster or to gravitational lensing, that increases the number of faint galaxies that are observed in the direction of the cluster through magnification effects. Emission from such galaxies can fill in the SZE decrement, leading to a wrong estimation of the effect. Galaxies inside the cluster are likely to affect the estimation of SZ effect at high frequencies while gravitational lensing effect is expected to be an issue for frequencies  $< 30$  GHz (Carlstrom, Holder & Reese 2002). The solution to this problem is increasing the resolution of the observations so that individual galaxies can be detected and accounted for; in low-resolution experiments such as Planck this will not be possible. The different frequency dependence of the SZ effect and galaxy emission will help to reduce contamination, but some residual effects will remain that can lead to additional unavoidable biases.

We remark that the method presented in this work is not incompatible with other SZ detection and estimation techniques. Linear filtering is an useful tool that can be used alone or as a step inside a more ambitious analysis of the data. The filters here introduced are computationally fast, robust, efficient and unbiased. They reduce the contamination due to noise and other astrophysical emission and optimise the separation between the thermal and the kinematic effect using all the frequency channels available (and not only the channels around the thermal crossover frequency). In the context of the future Planck mission, the implementation of the filters is straightforward, but due to the limitations on angular resolution and sensitivity the kinematic SZ effect will be badly determined. Experiments with more sensitivity and angular resolution will be much better for the detection of this elusive effect, but the implementation of the filters will require much more care since the inner structure of the clusters will reveal its complexity. We have hinted in the discussion some ways to deal with this complexity; applications to specific cases will be addressed in future works.

### ACKNOWLEDGMENTS

The authors thank Patricio Vielva for useful suggestions. DH acknowledges support from the European Community's Human Potential Programme under contract HPRN-CT-2000-00124, CMBNET, and the Instituto de Física de Cantabria for the hospitality during several research stays in 2003. RBB thanks the Spanish Ministerio de Ciencia y Tecnología and the Universidad de Cantabria for a Ramón y Cajal contract. MC acknowledges support from the Spanish Ministerio de Educación for a doctoral FPI fellowship. We thank FEDER Project 1FD97-1769-C04-01, Spanish DGESIC Project PB98-0531-C02-01 and INTAS Project INTAS-OPEN-97-1192 for partial financial support.

### REFERENCES

- Aghanim N., De Luca A., Bouchet F.R., Gispert R., Puget J.L., 1997, *A&A*, 325, 9.  
 Aghanim N., Hansen S.H., Lagache G., *A&A* submitted, astro-ph/0402571.  
 Bennett, C.L., et al. 2003, *ApJS*, 148, 97.  
 Birkinshaw M., 1999, *Physics Reports*, 310, 97.

<sup>2</sup> This is due to the same kind of effect that is the topic of this work: a cluster-like structure (in this case a "lump" of correlated galaxies with a correlation scale approximately equal to the cluster size) is superimposed to the observed cluster, showing a different frequency dependence but nevertheless producing a bias in the estimation of the cluster parameters.

- Broadhurst T. et al., ApJ submitted.
- Carlstrom J.E., Joy M.K., Grego L.E., Holder G.P., Holzzapfel W.L., Mohr J.J., Patel S., Reese E.D., 2000, *Physica Scripta*, T85, 148.
- Carlstrom J.E., Holder G.P. & Reese E.D., 2002, *ARA&A*, 40, 643.
- Diego J.M., Vielva P., Martínez-González E., Silk J., Sanz J.L., 2002, *MNRAS*, 336, 1351.
- Enßlin T.A. & Hansen S.H., *A&A* submitted, astro-ph/0401337.
- Haehnelt M.G. & Tegmark M., 1996, *MNRAS*, 279, 545.
- Hansen S.H., 2004a, *New Astronomy*, 9, 279.
- Hansen S.H., 2004b, *MNRAS* submitted, astro-ph/0401391.
- Herranz D., Sanz J.L., Hobson M.P., Barreiro R.B., Diego J.M., Martínez-González E., Lasenby A.N., 2002, *MNRAS*, 336, 1057.
- Herranz D., Sanz J.L., Barreiro R.B., Martínez-González E., 2002b, *ApJ*, 580, 610.
- Hobson M.P., Barreiro R.B., Toffolatti L., Lasenby A.N., Sanz J.L., Jones A.W., Bouchet F.R., 1999, *MNRAS*, 306, 232.
- Hobson M.P. & McLachlan C., 2003, *MNRAS*, 338, 765.
- Hu W. & White M., 1997, *ApJ*, 479, 568.
- López-Cañiego M., Herranz D., Barreiro R.B., Sanz J.L., *MNRAS* submitted.
- Naselsky P., Novikov D., Silk J., 2002, *MNRAS*, 335, 550.
- Rephaeli Y., 1995, *ApJ*, 445, 33. Novikov D., Silk J., 2002, *MNRAS*, 335, 550.
- Seljak U. & Zaldarriaga M., 1996, *ApJ*, 469, 437.
- Sunyaev R.A., Zel'dovich Y.B., 1970, *Comments Astrophys. Space Phys.*, 2, 66.
- Toffolatti L., Argüeso F., De Zotti G., Mazzei P., Franceschini A., Danese L., Burigana C., 1998, *MNRAS*, 326, 181.